NATIONAL AERONAUTICS AND SPACE ADMINISTRATION

AMES RESEARCH CENTER

* at the for 7th Symposium of Ballistic Missile and Space Technology, 27-29, August 1962 - Los Angeles, Calif.

UNSTEADY AERODYNAMIC LOADS ASSOCIATED WITH TRANSONIC BUFFETING OF SPACE VEHICLES*

By Charles F. Coe

INTRODUCTION

The unsteady aerodynamic loads associated with buffeting which result from pressure fluctuations that occur within regions of shock waves and/or separated flow recently have become of considerable concern. Areas of vehicle exposure to separation have been potentially enlarged by recent trends to payloads that are larger than upper-stage rockets, resulting in the so called "hammerhead-shaped" launch vehicle. To date, at least three space vehicles have failed during launch through the atmosphere, with buffeting considered as a probable contributory cause. However, whether buffeting has been the direct cause of these failures has never been definitely established. It has been recognized, though, that buffet loads could have been involved, and consequently that these unsteady loads should be considered along with other loads in the design of space vehicle structures.

Two possible approaches may be taken to cope with the buffet problem. First, the most direct, but not always possible approach, would be to use configurations which eliminate trouble areas on a vehicle by avoiding separated flows. Second, when other design considerations make the first approach impractical to the extent that the response of the vehicle to buffet loads cannot be ignored, then these loads must be predicted. Unfortunately, all the information necessary for a confident prediction is difficult to acquire; and uncertain assumptions are usually required as in references 1 and 2.

An extensive research program has been undertaken at Ames Research Center to investigate the buffet problem by studying the local steady and fluctuating pressures and also both the overall buffet loads and elastic response of models. Figure 1 shows the profiles of most of the models tested

to date, and illustrates the scope of the tests that have been conducted. Both rigid models and dynamic models are shown. Tests were conducted in the Ames 14-foot transonic wind tunnel.

Longitudinal distributions of steady and fluctuating pressures were measured on all the rigid models using from 10 to 30 pressure transducers mounted along the top centerlines. On those models, designated by the letter "L", distributions of unsteady loading were obtained by measuring the differential pressures between the top and bottom halves of the models. In addition, on these models, the time correlated summations of the differential pressures were obtained, taking into account the necessary area-moment weightings to give the unsteady bending moments about a selected point. From 40 to 100 pressure transducers were used. These rigid-model unsteady bending moments can then be correlated with the dynamic model results.

Tests of the dynamic models were performed using a dynamic balance to obtain the frequency response and also using an elastic support to measure the overall buffet response. These results are described in an accompanying paper by Mr. Henry Cole, Jr.

As can be seen in Figure 1, some of the models tested were specific configurations, such as Nimbus, Advent, and Ranger, but others were tested with some attempt to achieve a systematic variation of profiles to determine effects of nose bluntness, body convergence, and cone angle and cone bluntness. Scale effects have also been investigated by testing different sizes of models 8 and 13.

The intention of this paper is to summarize the results obtained to date from the rigid model tests. Some of the work has been published in the NASA TM's shown in the figure (references 3 and 4). Details of the model construction, test procedure, and instrumentation can be found in these references.

EFFECTS OF PROFILE GEOMETRY

Since consideration of the effects of variations in profile geometry could potentially lead to the elimination or reduction of buffet loads on a vehicle through proper selection of shape, these effects will be discussed first.

Figure 2 shows the longitudinal distribution of the pressure fluctuations measured along the top centerlines of two models which indicate the effects of nose bluntness. The results illustrate how buffeting loads on a cylindrical body can be significantly reduced by using a nose that is slender enough to avoid separation. On the model with the more slender nose, local pressure fluctuations are confined primarily to the region of the shock wave, whereas, if separation occurs (model with blunt nose) fluctuations occur over much of the body.

Figure 3 shows results from tests of a variation of cone angle and cone bluntness. Only two curves are shown, but they illustrate the primary differences that were found. The curve on the left shows pressure fluctuations that result from a pointed cone with a 20° half-cone angle. It can be noted that the cone-cylinder intersection angle is sharp enough that fluctuations due to separation occur. Since the pointed 20° cone appears unfavorable, it goes without saying that any blunting with this angle or further increase in cone angle would not give improvement. Results from tests with a pointed cone having a 15° half-cone angle showed that separation effects were virtually eliminated, and that blunting the cone with a hemisphere to the degree shown on the right of the figure had no adverse effect. The figure shown is for the most blunt hemisphere-cone combination tested which had a fineness ratio of approximately 0.8. It was found that there was little effect of blunting the cone on the intensities of the pressure fluctuations up to the degree of bluntness shown. Blunting back to a hemisphere did result in high-level fluctuations due to separation, however.

The effects of body convergence are illustrated in figures 4 and 5. Figure 4 shows that for moderate convergence, fluctuations are low at α=o with the exception of those confined to the region of the shock wave. However, with increasing angle of attack, separation effects appear and considerable area can be exposed to fluctuations. The Mach number range over which pressure fluctuations occur extends from approximately 0.8 to 1.0. Figure 5 shows that when body convergence is made sharper, fluctuations occur within separated regions which are independent of the shock wave, and that they persist to supersonic speeds, potentially extending through the maximum "q" condition during a vehicle launch. From these rigid model results, it would appear that gradual boattailing is more desirable than the step, but additional factors that are evident from the dynamic model tests must be considered. These factors will be described in the previously mentioned accompanying paper by Mr. Cole.

POWER SPECTRAL DENSITIES

Power spectral densities of the pressure fluctuations have been measured for many of the models, and generally it has been found that the shapes of power spectra depend upon the type of flow on a body and the location within the type of flow rather than upon the specific profile. Figure 6 shows representative power spectra to indicate the limits of the shapes. The curve which shows the lower frequency concentration of energy is typical of the shapes obtained from pressure fluctuations in the region of a strong shock wave and from fluctuations near the forward boundaries of separated flows. The shape of the power spectrum changes to one which is relatively flat with frequency as the distances from the forward boundary of the separation to the measurement station is increased. The flat power spectrum is also typical for flow in the region of the shcok wave when the shock wave is beginning to form on a body, and is flat for the case when separation is independent of the shock wave following a sharp boattail angle or step.

SPACIAL CORRELATION OF PRESSURE FLUCTUATIONS

If it becomes necessary to predict the response of a vehicle to unsteady pressures, the spacial correlation of these fluctuations must be measured or estimated with some confidence so that proper phasing of the local pressures can be applied. Some work by R. E. Bieber of Lockheed, shows at least an order of magnitude range of estimated response of a vehicle depending upon whether zero correlation or unity correlation is assumed. The only alternative to determining the spacial correlation would be to apply pressure-transducer summing techniques or possible resonance compensation techniques to yield total rigid model unsteady loads directly. As previously mentioned, direct summation of pressure transducers has been applied to some of the rigid models of this investigation for coordinated tests with the dynamic models.

Figure 7 shows the normalized co-power and quadrature-power of the cross spectra between differential pressure-fluctuation measurements from model 11. This model was a 10 percent scale model of the Advent-Agena configuration without any external protuberences. Each plot shows the cross spectra between the fluctuations at the stations indicated and the reference station. The results show that the decay of time or phase related energy over a longitudinal distance varies with frequency. At 25 c.p.s., for example, which corresponds to a scaled frequency near the first bending mode of the full scale vehicle, the reduction of the in-phase components amounts to an approximate exponential decay to 1 percent of its maximum value in a distance of about 4 Agena diameters. On the other hand, at the frequency corresponding to the estimated second bending mode of the vehicle, 78 c.p.s., it is apparent that a similar decay occurred in a much shorter distance.

It would be nice to be able to report that the longitudinal correlation of differential pressures on model 11 is typical for separated flow. To examine the results for a different profile on which there was flow separation,

figure 8 shows some cross spectra measurements from model 8. Unfortunately, the arrangement of transducer stations on the taped records did not provide for time correlation of the fluctuations over much of the model length, however, the results shown are sufficient to illustrate that the longitudinal correlation can vary with profile. The results suggest a greater degree of correlation of pressure fluctuations on a boattailed body with moderate convergence than on a body with sharper boattailing. It is interesting to note here that the dynamic model 8 (a) exhibited an instability and large dynamic response.

The manner in which the pressure transducers were connected in the circuits to give differential pressures did not allow cross-spectra measurements between top and bottom or peripheral pressures. However, figure 9 shows a comparison made between the root-mean-square pressure fluctuations along the top centerline of model 11 and the differential pressure measurements. The results are from the separated flow region only. A fairly consistent trend is shown which indicates that the differential pressure fluctuations were approximately 50 percent greater than the top centerline fluctuations for a case where the separated flow completely surrounded the body.

SCALE EFFECTS

As previously mentioned in the description of model profiles, some work was also undertaken to briefly look into the effects of scale.

Figure 10 shows the pressure fluctuations on model 13 for three different model sizes which corresponded to 10 percent, 25 percent, and 43-1/3 percent of full scale of an Agena-Atlas vehicle. The two smaller models were sting supported, and the larger model was a half model mounted on the wall of the wind tunnel to reduce possible blockage effects. The effects on the pressure fluctuations within the separated flow region shown for M=0.84 are typical of the results for Mach numbers below 0.84; that is, there was some difference between the 10 percent and 25 percent models, but no further change between the 25 percent and 43-1/3 percent models. The inference is that there is a minimum size limit of models which can be depended upon for quantitative information. At Mach numbers nearer 1.0, there was a further increase in the pressure fluctuations on the 43-1/3 percent model, however, steady pressures were not duplicated in the separated flow region, possibly due to the increased thickness of the wind tunnel wall boundary layer, consequently, conclusions cannot be drawn.

Since the power spectral densities of the pressure fluctuations in the separated flow on model 13 were relatively flat for all the model sizes, conclusions in connection with frequency scaling could not be drawn from this model. To check the constant Strouhal number concept then of scaling frequencies, two sizes of model 8 were tested since the power spectra of the fluctuations in the region of the converging section were not flat. The model sizes corresponded to 14 percent and 22 percent of full-scale based on an Agena diameter. Figure 11 shows both the RMS values and a comparison of the spectra at the model station indicated. Although the power spectral densities do not indicate perfect agreement for all reduced frequencies, the trends favor the validity of scaling frequencies by constant Strouhal number.

The RMS values agreed favorably for these two model sizes up to a Mach number near 0.96. Above this Mach number, the flow attached on the smaller model but remained separated on the larger model up to the highest test Mach number of 1.05. This result suggests a possible effect of scale on the Mach number boundaries of buffeting.

In addition to the model size variations to investigate scale effects, some tests were also conducted with model 8 in the Ames 11-foot transonic wind tunnel at various tunnel total pressures. Figure 12 shows the power spectra of differential-pressure fluctuations at total pressures from 15 inches of mercury to 60 inches of mercury. The curves have been normalized to the 30-inch pressure level. As can be seen, scale effects in-so-far as variations in total pressure are concerned are not pronounced.

CONCLUDING REMARKS

In conclusion, the results of this investigation have shown that the unsteady aerodynamic loads associated with buffeting can be largely eliminated if "hammerhead" configurations could be avoided, and if cone-cylinder intersection angles of 15° or less could be used. A conical nose with a 15° half-cone angle can be blunted to 8-tenths of the cone base diameter without introducing separation effects. Unfortunately, it is not always practical to use a vehicle with a"minimum buffet" configuration, so it becomes necessary to add to the other structural loads that occur during launch those that are estimated due to buffeting. This estimation must take into account both the rigid model characteristics plus the effects of motion.

REFERENCES

1. Goldberg, A. P. and Wood, J. D.: Dynamic Loads in the Atlas-Able 5 During Transonic Buffeting. STL/TM-60-000-19075, 22 August, 1960.
2. Goldberg, Arthur P. and Adams, Richard H.: Mercury-Atlas Buffeting Loads at Transonic and Low Supersonic Speeds. STL/TR-60-0000-AS431, 28 November, 1960.
3. Coe, Charles F.: Steady and Fluctuating Pressures at Transonic Speeds on Two Space-Vehicle Payload Shapes. NASA TM X-503, 1961.
4. Coe, Charles F.: The Effects of Some Variations in Launch-Vehicle Nose Shape on Steady and Fluctuating Pressures at Transonic Speeds. NASA TM X-646, 1961

Figure 1

PROFILES OF MODELS TESTED

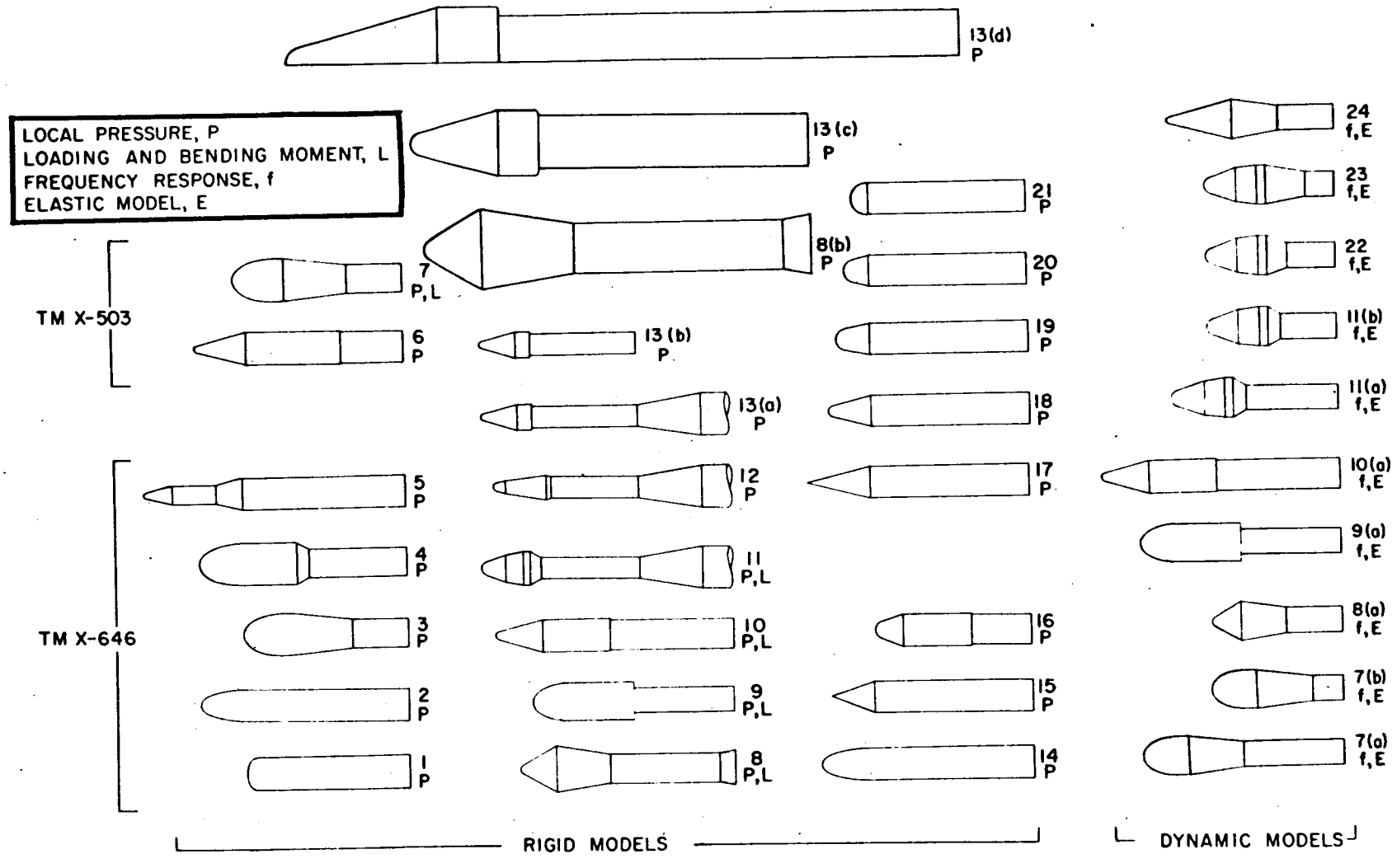

Figure 2

EFFECT OF NOSE BLUNTNESS

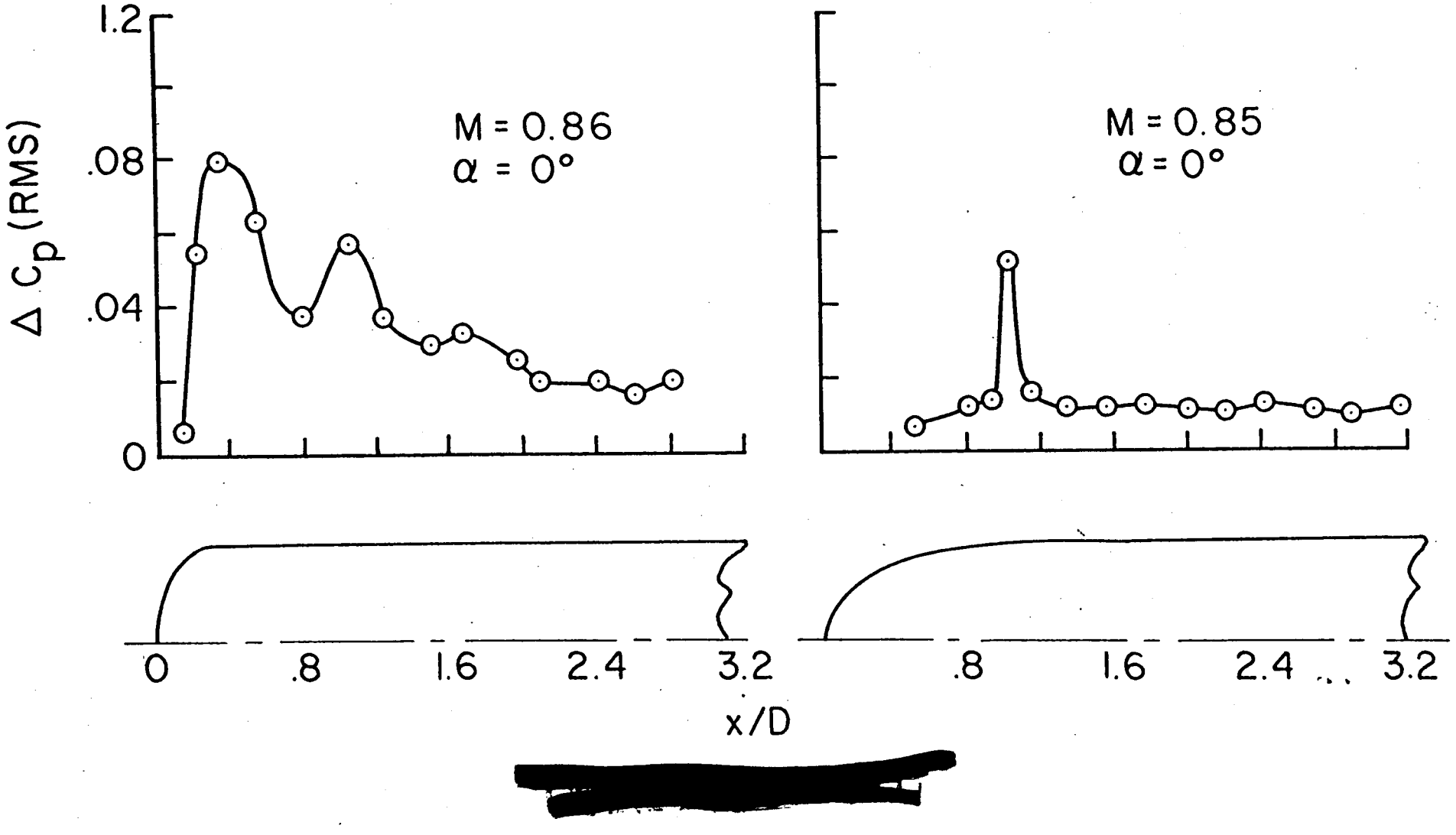

Figure 3

EFFECT OF CONE ANGLE AND CONE BLUNTNESS

M = 0.89, $\alpha = 8°$

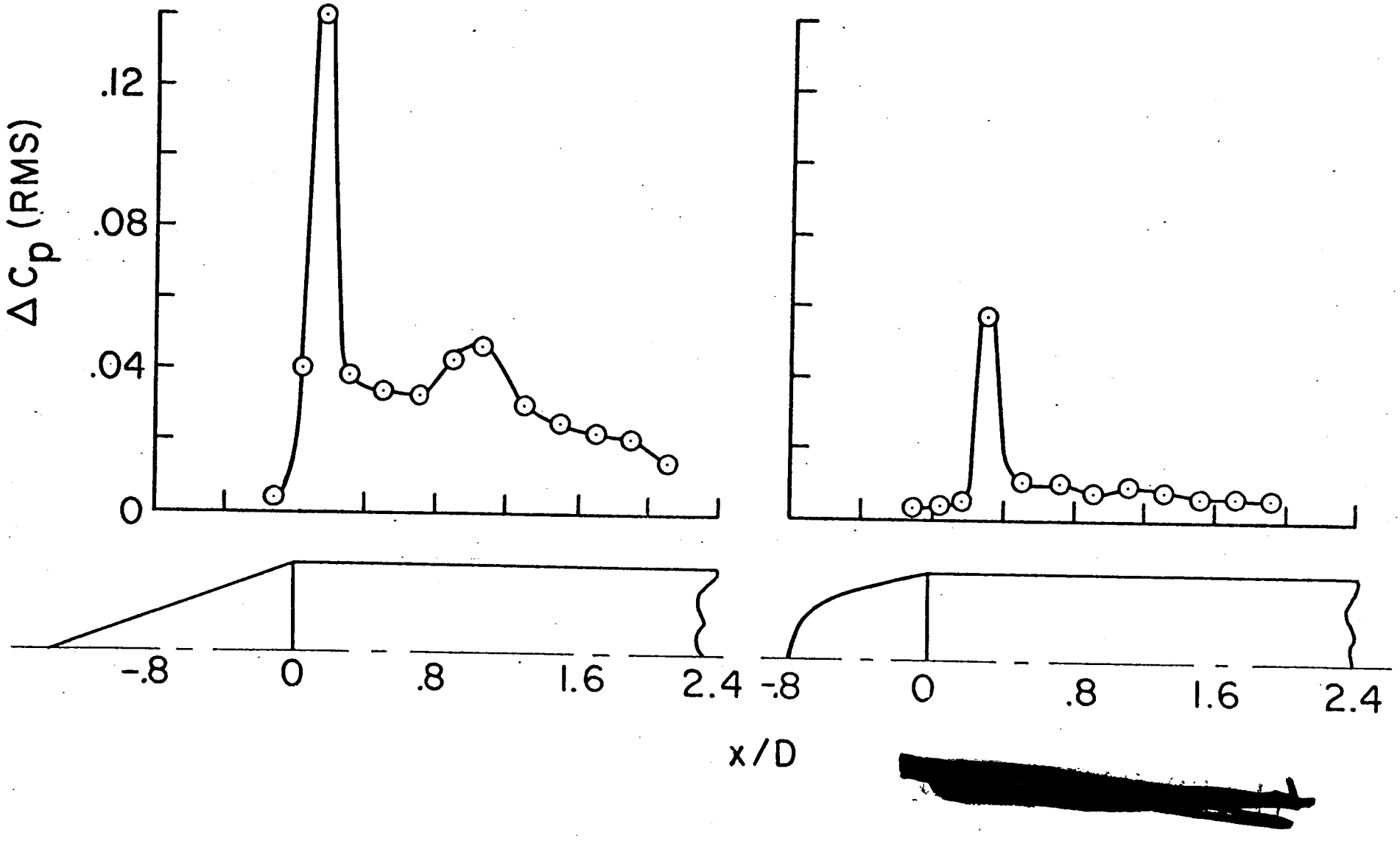

Figure 4

EFFECT OF BODY CONVERGENCE ANGLE OF ATTACK

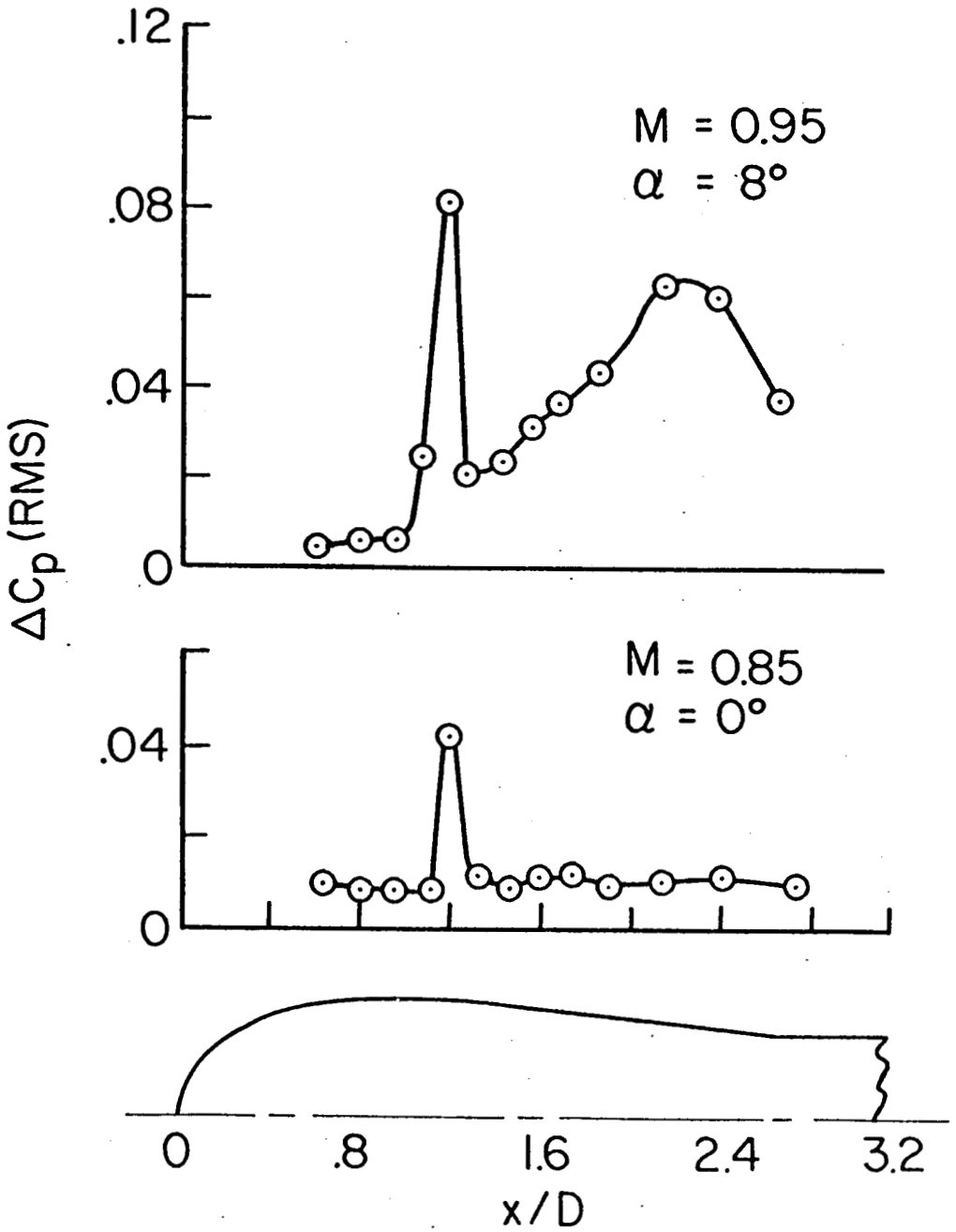

Figure 5

EFFECT OF BODY CONVERGENCE MACH NUMBER

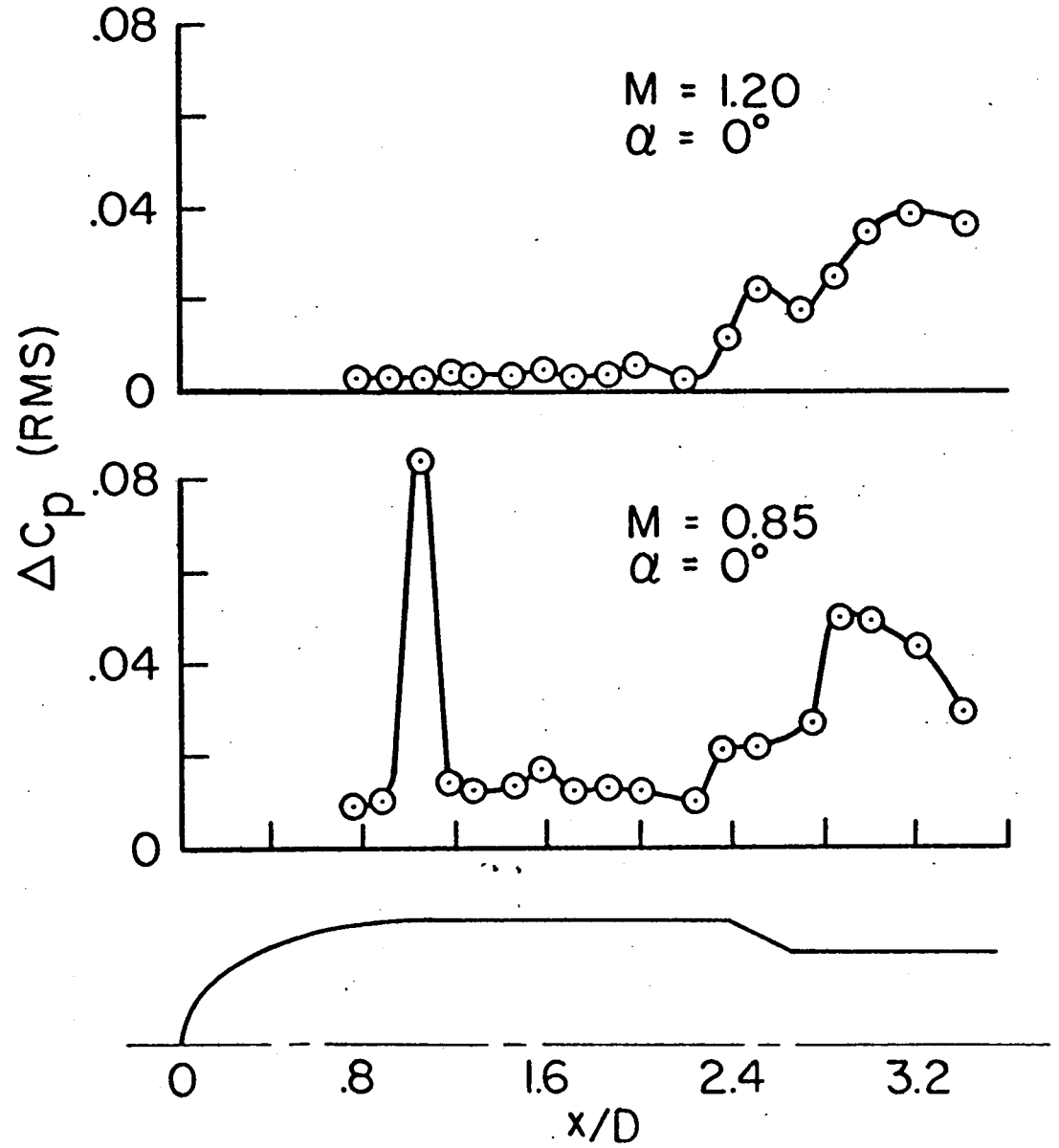

Figure 6.- REPRESENTATIVE POWER SPECTRA

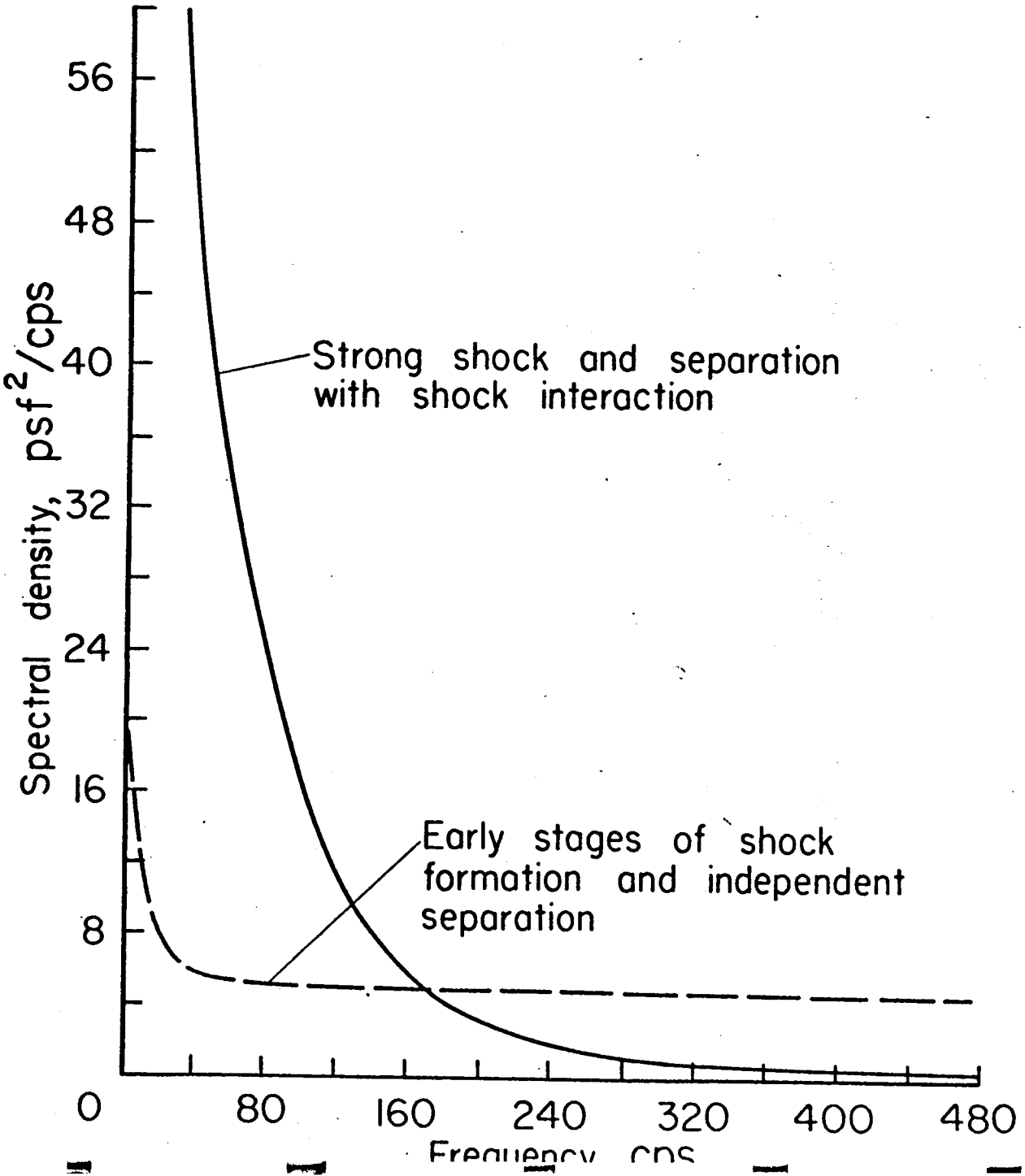

Figure 7

LONGITUDINAL CORRELATION OF DIFFERENTIAL PRESSURE

MODEL 11, $M = 0.95$, $\alpha = 0°$

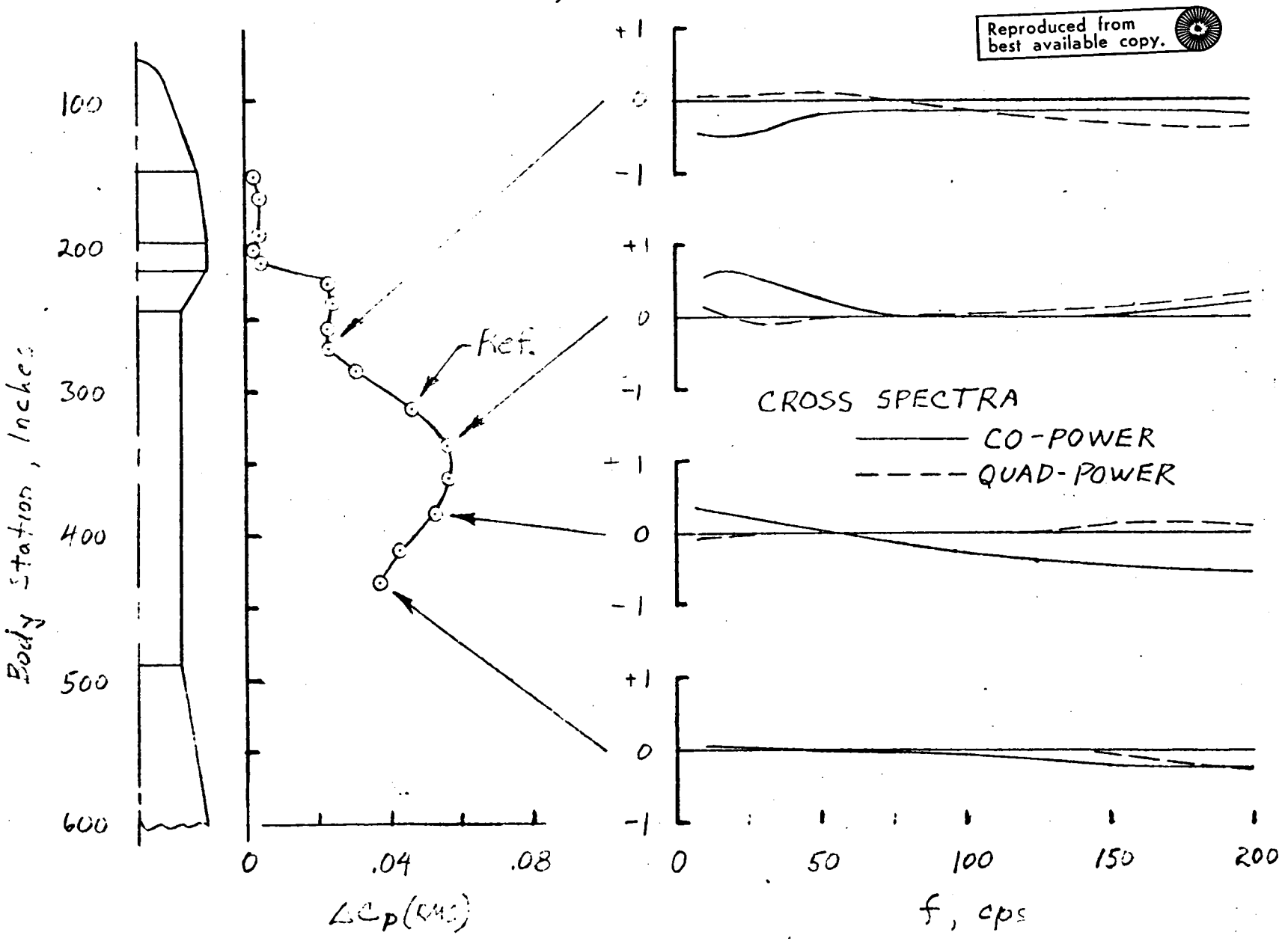

Figure 8

LONGITUDINAL CORRELATION OF DIFFERENTIAL PRESSURE

MODEL 8, $M=0.90$, $\alpha=0°$

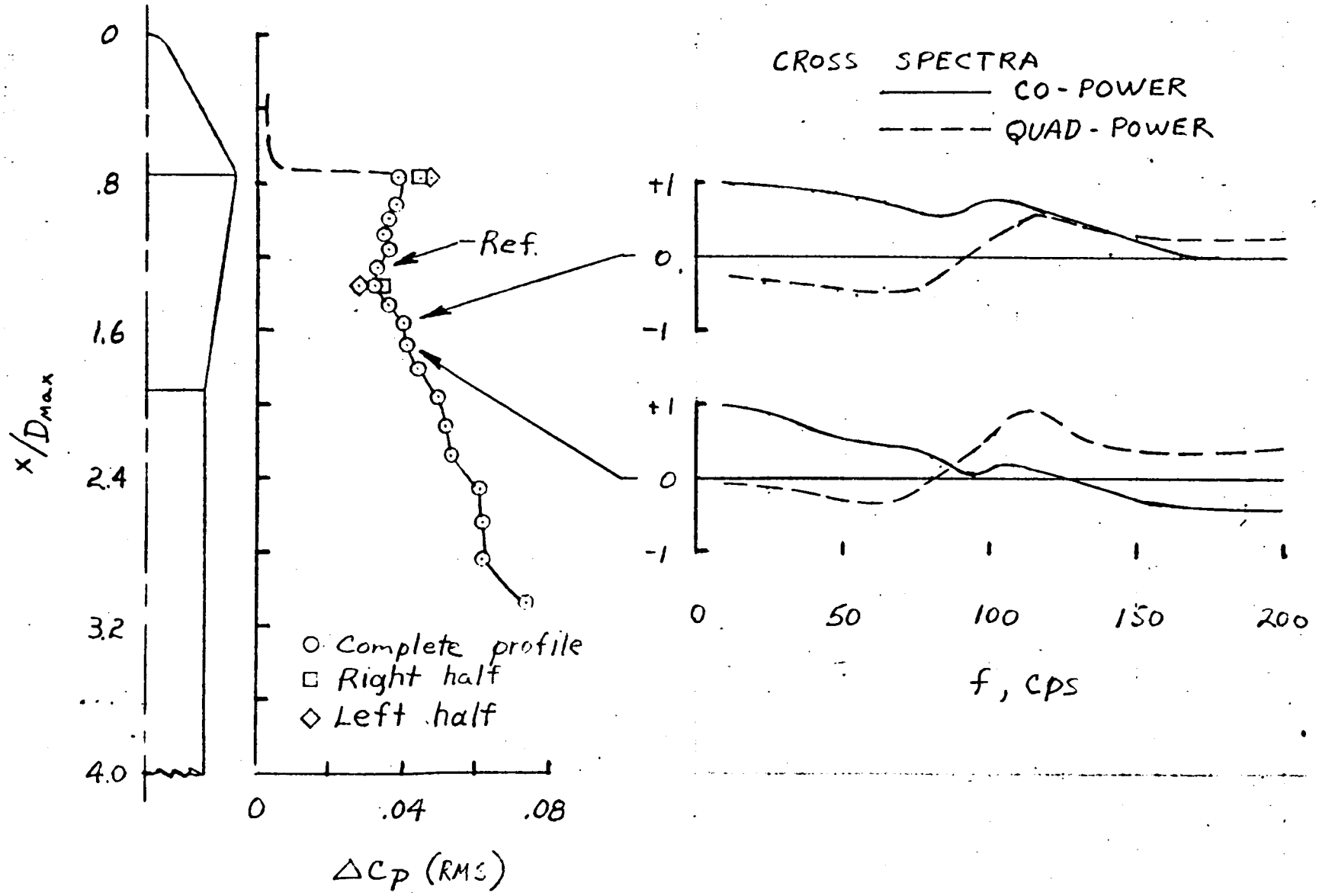

[redacted]

Figure 9

RELATIONSHIP BETWEEN TOP CENTERLINE AND DIFFERENTIAL PRESSURE ON MODEL II

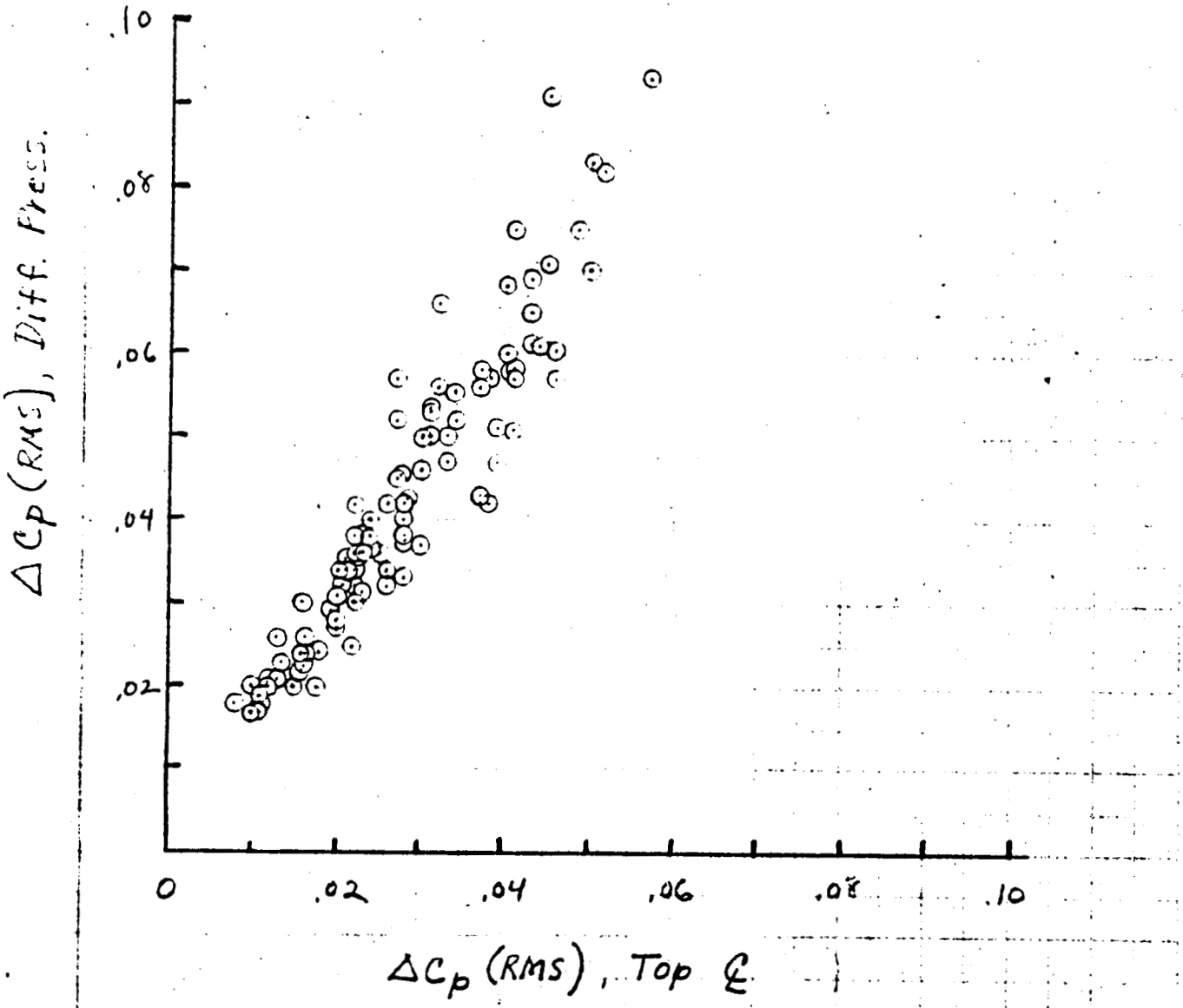

[redacted]

[redacted]

Figure 10

EFFECT OF SCALE ON MODEL 13
$\alpha = 0°$

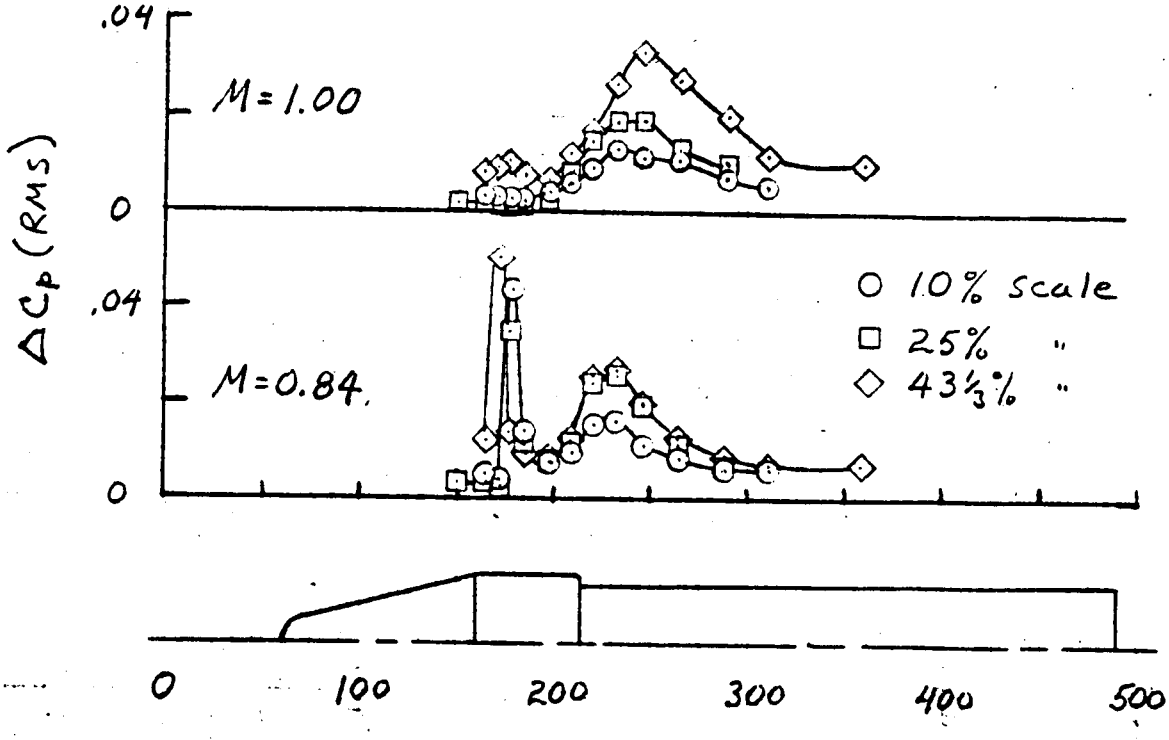

[redacted]

Figure 11

EFFECT OF SCALE ON MODEL 8

$M = 0.90$, $\alpha = 0°$

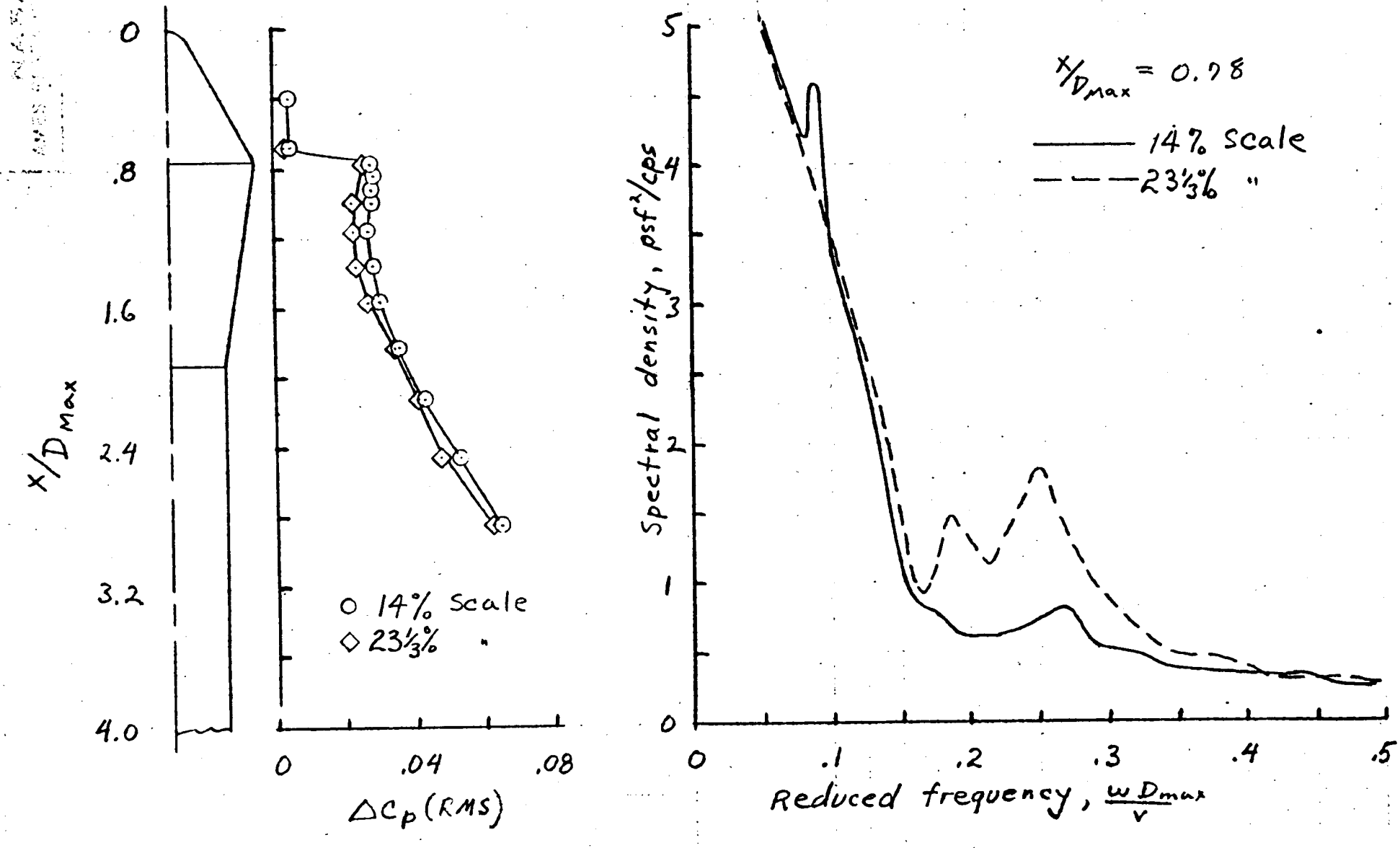

Figure 12

EFFECT OF TOTAL PRESSURE